Eur Biophys J (2011) 40:281–288
DOI 10.1007/s00249-010-0646-3

ORIGINAL PAPER

Dielectrophoretic stretching of cells allows for characterization of their mechanical properties

Isabella Guido · Magnus S. Jaeger · Claus Duschl

Received: 31 August 2010 / Revised: 8 November 2010 / Accepted: 12 November 2010 / Published online: 26 November 2010

Abstract The mechanical behavior of biological cells is mainly determined by the cytoskeleton. Its properties are closely interlinked with many cellular events, including disease-related processes, and, thus, may be exploited as potent biomarkers. We have stretched two types of cells between microelectrodes through the application of dielectrophoretic forces. Small numbers of cells of cancerous origin (MCF-7) and from related noncancerous tissue (MCF-10A) were sufficient to obtain data that allowed us to unambiguously distinguish these cells. The Maxwell tension applied has been estimated to be 56 Pa. A detailed analysis of the cells showed that the differences in the stretching response are due to cell-specific mechanical properties. Through the addition of an actin- and a microtubule-specific toxin to the cells, differences in the microtubular structures of the two cell types have been identified as the major cause for the behavior observed. Our approach shows enormous potential for parallelization and automation. Hence, it should be suitable for achieving throughputs that make it attractive for many biomedical diagnostic purposes.

Keywords Dielectrophoresis · Cytoskeleton · Deformation · Stiffness · Microelectrodes

I. Guido · M. S. Jaeger (✉) · C. Duschl
Fraunhofer Institute for Biomedical Engineering (IBMT),
Am Muehlenberg 13, 14476 Potsdam, Germany
e-mail: magnus.jaeger@ibmt.fraunhofer.de
URL: www.ibmt.fraunhofer.de

Introduction

The way in which cells respond to the application of external force seems to depend, in many examples, strongly on their type, on their particular state during differentiation and proliferation, and on disease-related degeneration or other aberrations. The architecture that determines this response is the cytoskeleton, which consists of three main types of filaments: actin, intermediate filaments, and microtubules. The organization and density of these building blocks not only determine the shape and the rigidity of the cell, but they are also actively involved in cellular processes, such as migration, cytokinesis, and the intracellular transport and distribution of organelles. The status of a cell is the result of highly interrelated processes with complex feedback control loops. For example, the expression of proteins correlates with particular mechanical parameters. Thus, these parameters may serve as meaningful biological markers for the characterization of cells. The cytoskeleton spans almost the entire cell. Therefore, it is expected to provide global information about the cell status. This is in contrast to molecular markers, which are specific to particular processes. Another benefit of characterizing cellular mechanical properties is that their determination is performed with live cells without the necessity of carrying out laborious staining or pretreatment protocols. Hence, the screening of cells based on mechanical properties, optionally in combination with the detection of molecular markers, may prove advantageous in many scenarios in biomedical research, for diagnostic purposes, and in drug development.

In recent years, a number of experimental techniques have been developed with the aim of assessing mechanical properties of living cells at different length and time scales. These techniques provide information from the

submicrometer scale, such as atomic force microscopy (AFM, Binnig et al. 1986; Henderson et al. 1992; Radmacher et al. 1996; Rotsch and Radmacher 2000; Van Vliet et al. 2003) and magnetic twisting cytometry (MTC, Wang et al. 1993; Puig-De-Morales et al. 2001), to the cell population level, such as cell-populated gels or sheared cell monolayers (Brown 2000). At the single-cell scale, important examples include micropipette aspiration (Hochmuth 2000), optical tweezers (Lim et al. 2004), microplate rheometer (Thoumine et al. 1999), optical stretcher (Guck et al. 2001), and bulge generation method (Kim et al. 2007). The micropipette aspiration (Evans 1973) and the optical tweezers (Dao et al. 2003; Hénon et al. 1999; Mills et al. 2004) were successfully used for studying the mechanical properties of red blood cells. The optical stretcher (Guck et al. 2005), the bulge generation method (Kim et al. 2008), and the microplate rheometer (Thoumine and Ott 1997a, b) as well as AFM (Li et al. 2008) were used more recently for the analysis of cancer cells. It was shown that these devices are able to distinguish malignant cells from nonmalignant counterparts. The bulge generation method, the microplate rheometer, and the AFM-based approach allow for highly precise quantification of the force generated. However, these techniques are not easily compatible with the demand of processing cells with high throughput and in a nondestructive manner that allows for subsequent cell analysis. The optical stretcher approach overcomes these limitations. Cells get stretched in two nonfocused laser beams that propagate in opposite directions. The method has been demonstrated to provide data on the viscoelastic properties of cells at a considerable processing speed. The information obtained can be used to distinguish cells according to various biomedically relevant criteria.

Here, we present an alternative approach for the analysis of the mechanical properties of cells. It makes use of the forces that act on cells when exposed to high-frequency electric fields. After the pioneering work into the viscoelastic properties of erythrocytes by the group of Sackmann (Engelhardt et al. 1984), dielectrophoresis has mainly been used in recent years for positioning and directing cells. In our approach, we make use of the progress that has been achieved during this time with respect to the integration of electrodes into microsystems, such as lab-on-chips (Pethig and Markx 1997). It is this aspect where we believe that our approach shows valuable advantages over its optical counterpart: microelectrodes can now easily be processed in microfluidic environments at comparatively low costs. Together with the low energy demands for driving the electrodes, this feature enables highly parallel processing. Here, the optical stretcher has its limitations. Although the optical fibers for guiding the light to the cells are also compatible with microfabrication, the laser power required to stretch cells is considerable. Hence, the operation of parallel cell processing channels would require the installation of high-performance laser equipment. Another favorable aspect of our approach is that it can easily be combined with dielectrophoretic manipulation units for aligning, sorting, or positioning of cells, such that entire cell processing lines can be established in a chip format.

In this paper, we evaluate the method by mechanically deforming two closely related and well-characterized adherent cell lines (An et al. 2009). MCF-10A is a nontumorigenic epithelial cell line that has been derived from benign breast tissue affected by fibrocystic disease. The origin of the corresponding MCF-7 cells is human adenocarcinoma tissue. This pair of cells was chosen to have a cell system available whose mechanical properties have already been investigated. However, the MCF-10 cells studied by others are suspension cells (MCF-10F, Guck et al. 2005). We believe that our choice represents a more suitable pair of cells as both cell types are adherent. By chemical modification of the cytoskeleton, we identified the components that are responsible for the differences in deformability between cancerous and noncancerous cells (Tuszyński et al. 1997). Numerical calculations of the electric field provide a comprehensive picture of how the electric field acts on the cells.

Materials and methods

Cells

Human breast adenocarcinoma cells (MCF-7) were kindly donated by Robert Clarke, University of Manchester, UK. The human nontumorigenic epithelial cell line MCF-10A derived from benign breast tissue with fibrocystic disease was obtained from American Type Culture Collection (Rockville, MD, USA). MCF-7 cells were cultivated under 5% CO_2 in standard glucose Dulbecco's Modified Eagle Medium (DMEM, Gibco Invitrogen, Carlsbad, CA, USA) supplemented with 10% fetal bovine serum (Biochrom, Berlin, Germany). MCF-10A cells were cultivated under 5% CO_2 in DMEM/F12 supplemented with 5% horse serum, 0.5 μg/ml hydrocortisone, 10 μg/ml insulin, 20 ng/ml EGF, 0.1 μg/ml cholera toxin, 2 mM glutamine, and 1% penicillin/streptomycin (Ahn et al. 2004; Kim et al. 2005; Martin and Leder 2001).

Prior to the experiments, both cell types were harvested by trypsination (MCF-7: trypsin/EDTA 0.25/0.02%, 13 min; MCF-10A: trypsin/EDTA 0.05/0.02%, 10 min). The different trypsin concentrations did not contribute to the subsequent differences in stretching, as was verified in control experiments by comparing the effect of both concentrations on MCF-10A cells (not shown).

For the stretching measurements, cells were resuspended in an isotonic solution (Cytocon Solution I, Perkin Elmer, Hamburg, Germany). This commercially available aqueous polymer solution effectively reduces undesirable nonspecific adhesion of the cells to the microchip surfaces. In preceding measurements, no adverse effects of the solution on cell function were observed. Though this non-stick solution facilitates the experimental work, it is by no means compulsory. The electric conductivity σ_e was adjusted to 5 mS/m by mixing with 0.3 M inositol solution and phosphate-buffered saline (703 Laboratory Conductivity Meter, Knick, Berlin, Germany). Thus, the electric conductivity could be changed without affecting the osmotic pressure. In principle, any medium may be used, as long as its electric conductivity stays below that of the cells. Note that during the experiments, the cells were always used in suspension.

Microchips

The microchips employed in the experiments consisted of planar arrangements of two microelectrodes with a width of 250 µm each and separated by a gap of 20 µm (cf. Fig. 2a). They were fabricated by structuring indium tin oxide-plated glass slides (20×20 mm^2, Schott, Gruenenplan, Germany) using UV ablation with a pulsed KrF laser at 248 nm (Lextra 100, Lambda-Physik, Goettingen, Germany). Fluidic access was achieved by mounting a silicone trough onto the processed slides, forming a sample volume of roughly 200 µl.

Image acquisition

Optical microscopy was performed using a microscope with a 20×/0.35 objective (BX40, Olympus, Hamburg, Germany). For recording, a computer-controlled CCD camera was employed (Orca ER, Hamamatsu Photonics). The camera was controlled by a program provided by the camera manufacturer (Simple-PCI). The frame rate of the CCD camera was nine digitized frames per second with 640×512 pixels^2 in eight-bit resolution. The extension of the cells along the direction of force, i.e., perpendicular to the electrode edges, was measured manually every 2 s during the first 10 s and every 5 s afterwards (Image-Pro Plus 4.0, Media Cybernetics). Although in general the difference in deformation was already clearly discernable after 10 s (cf. Fig. 2b), the measurements were continued for a whole minute to (a) not miss plateaus and (b) provide comparability by fitting with existing mechanical models (see "Results"). The measure always coincided with the long axis of the ellipsoidal cells during stretching. Their elastic properties were assumed to be isotropic. All measurement data are given as mean with the number n of analyzed cells and error bars indicating the SEM. Statistical significance levels were calculated with t tests performed between data sets obtained at identical time points after onset of stress and are given as the probability of error p.

Dielectrophoresis

Cells are dielectric particles that become polarized in an electric AC field (Pethig 1979). When the cells interact with an inhomogeneous electric field, they experience forces that may lead to translational motion called dielectrophoresis (DEP), to electrorotation, or to their elongation and stretching (Pohl 1978; Gimsa et al. 1991; Sukhorukov et al. 1998). The magnitude of the force depends on the dielectric properties of the cell with respect to those of the medium and the size of the object. The sign of the contrast between the dielectric properties of the particle and the medium determines the direction of the force. As the dielectric properties of the particle (and to a much lesser degree of the medium) depend on the frequency, this parameter can be used to preset the direction of the force. Elongation is achieved when the polarizability of the particle exceeds that of the surrounding medium (Thom and Gollek 2006). In this configuration, the translational force points in the same direction as the field gradient, typically towards the electrodes (positive DEP or pDEP). The repulsion of the particle from the regions of high field strength is called negative DEP (nDEP). The parts of a spectrum where positive and negative DEP occur are separated by crossover frequencies where no polarization charges are induced (Ermolina and Morgan 2005).

The stretching experiments were performed by feeding the microelectrodes with a square waveform signal of $f_{\mathrm{exp}} = 15$ MHz and 6 V_{rms} using a function generator (33120A, Agilent). The analysis of an equivalent circuit of the cell membrane at this frequency reveals that the membrane is capacitively bridged, such that the electric conductivity of the cytoplasm predominantly determines the level of polarization charge generation and, hence, the force field (Sukhorukov et al. 1998). Consequently, pDEP occurs, the cells get trapped near the electrode edges and are subsequently stretched by the electric field there. The opposite of all three effects would occur at insufficiently high frequencies. The high frequency also served to effectively prevent electrochemical degradation, e.g., of the electrodes. Trapping of the cells at the electrodes was carried out at 2 V_{rms} at the same frequency. Applying this voltage did not cause any measurable deformation.

Simulation and fitting

For the finite element simulation, we used the Quasi-Statics Electric package from the Electromagnetics

Module of Comsol Multiphysics 3.2 (Comsol, Stockholm, Sweden). For this, the medium relative permittivity was set to 78.69 and its electric conductivity to 5 mS/m. Curve fitting was performed using Mathematica 7.0.0 (Wolfram Research).

Results and discussion

This section consists of the description of two experimental approaches: in the first part, force-dependent deformation experiments using MCF-7 and MCF-10A cells are reported. In the second part, experiments that explore the interaction of filament-specific chemical compounds with the cytoskeleton are used to identify the causes for the differences in response between the two cell types.

A comprehensive description of the deformation experiments requires a reasonable estimation of the forces applied. As there is no available way to determine the forces directly, we made use of considerations that have been applied to a related problem, namely the stretching of erythrocytes in an electric field (Engelhardt and Sackmann 1988); the Maxwell tension π is determined using

$$\pi = \frac{9}{4}\varepsilon\varepsilon_0 E^2 \cos^2\theta \quad (1)$$

with ε and ε_0 being the dielectric permittivity of the medium and the vacuum, respectively, and θ the angle to the electric field (i.e., stretching) direction. The simplifications applied in this approach are also valid in our work, namely that the force is independent of the frequency and dissipative effects can be neglected. We comply with the first

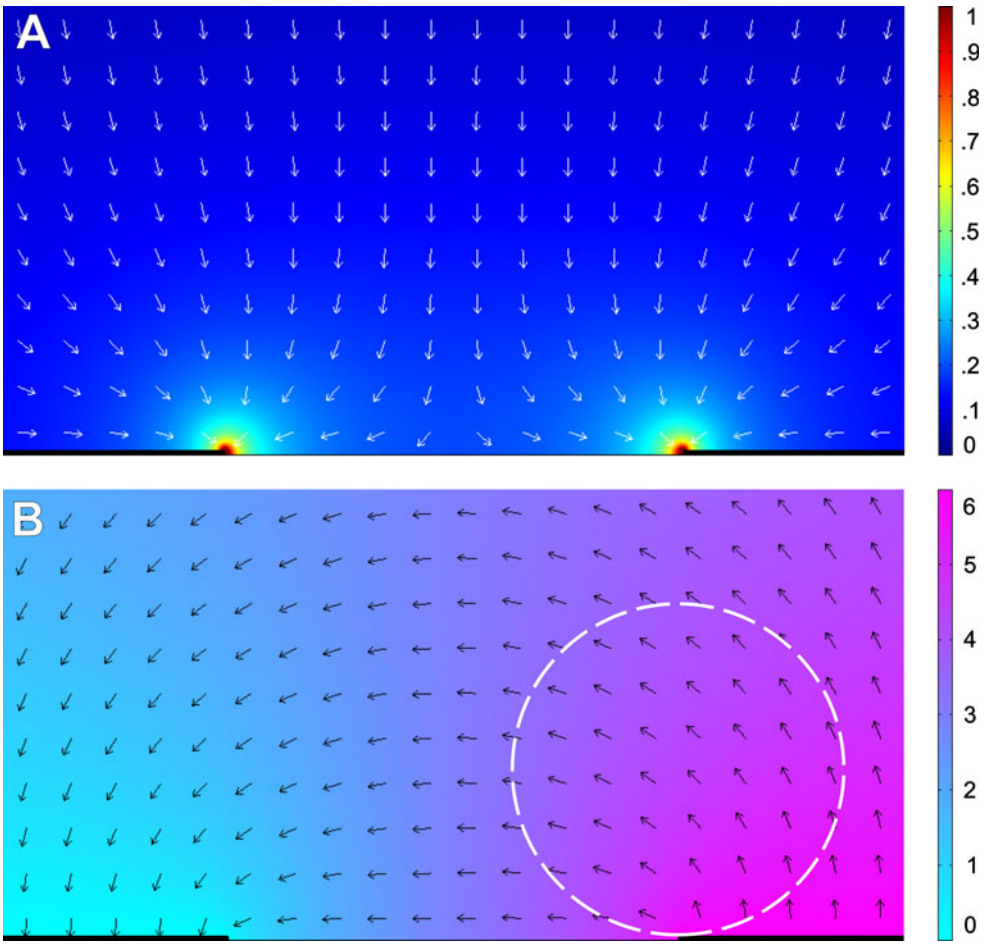

Fig. 1 Finite element simulation of the electric field in the microchip. The electrodes are depicted by the *black bars* at the *bottom* of the drawings. **a** The *arrows* indicate the direction of the dielectrophoretic force that transports the cells to the nearest electrode edge. The *background colors* indicate the electric field strength given in V/μm. In a homogeneous case, the conditions chosen (6 V, 20 μm) would yield 0.3 V/μm. **b** The *arrows* show the direction of the electric field between the microelectrodes. The electro-deformation that a cell undergoes after having been trapped dielectrophoretically at the edge of one microelectrode occurs along these field lines. The outline of a cell (before deformation) is indicated for size comparison (*white dashed circle*) at the typical trapping position. With equal probability, the cell might have been trapped at the other electrode (cf. Fig. 1a) and would thence be stretched, again along the field lines, into the opposite direction. The *background coloring* codes the electric potential (given in volts)

assumption by employing a frequency in the stretching experiments that was sufficiently different from the cross-over frequencies (Castellarnau et al. 2006; Schnelle et al. 1999). The electric field E was calculated numerically and integrated over the volume of the initially spherical cell (see Fig. 1). For a voltage of 6 V, we estimated the Maxwell tension π to be approximately 56 Pa at maximum, i.e., along the stretching direction ($\theta = 0$).

Figure 2 summarizes the results of step stress experiments on MCF-7 and MCF-10A cells. The cells were trapped at the electrodes through pDEP by applying a voltage of 2 V. This voltage is too low to induce any visible deformation. Then, a step stress was generated that was induced by increasing the voltage to 6 V for 60 s. The relaxation process was recorded for another 60 s. The two response curves (Fig. 2b) confirm what can already be deduced from the six micrographs (Fig. 2a), namely that the strain response ($\varepsilon = \Delta l/l_0$) of the MCF-10A cells, i.e., the noncancerous cells, is approximately two and a half times stronger than that of the MCF-7 cells derived from a human adenocarcinoma. The noncancerous cells appear considerably softer than the related cells from the cancer cell line. This is in contrast to findings obtained through optically induced stretching (Guck et al. 2005). However, communication with this group revealed that the conditions used as to time scale and strain range are too different to allow direct comparison of the outcome.

In both MCF-7 and MCF-10A cells, a fast increase in the strain is followed by a regime showing a considerably slower increase after 8–10 s. In this regime, viscous behavior becomes more prominent. In order to relate our response curves to previous work, fits to the experimental data obtained during force application have been performed. As a fitting function

$$\varepsilon(t) = \left(1 - e^{-t/\tau}\right)p + qt \qquad (2)$$

has been chosen, since it is equivalent to solutions (Wottawah et al. 2005) of the constitutive equation used in Park and Scapery (1999). In spite of the considerable deformation, the data are fitted excellently by the model (Fig. 2b). The response time τ is similar for both cell types ($\tau_{\text{MCF-10A}} = 6.0 \pm 1.0$ s, $\tau_{\text{MCF-7}} = 5.3 \pm 0.8$ s) while p and q differ quite considerably: $p_{\text{MCF-10A}} = 8.0 \pm 0.7 \times 10^{-2}$, $p_{\text{MCF-7}} = 2.4 \pm 0.3 \times 10^{-2}$ and $q_{\text{MCF-10A}} = 1.2 \pm 0.2 \times 10^{-3}\ \text{s}^{-1}$, $q_{\text{MCF-7}} = 0.5 \pm 0.1 \times 10^{-3}\ \text{s}^{-1}$. The relaxation part of the curves shows that 50% of the strain relaxes in the case of MCF-10A cells and approximately 70% in the case of MCF-7 cells. In order to obtain additional information on the relaxation behavior, the strain has been measured as a function of a stepwise increase of the voltage applied, followed by an unload phase (Fig. 2c). The duration of each voltage step (1 V) during the loading

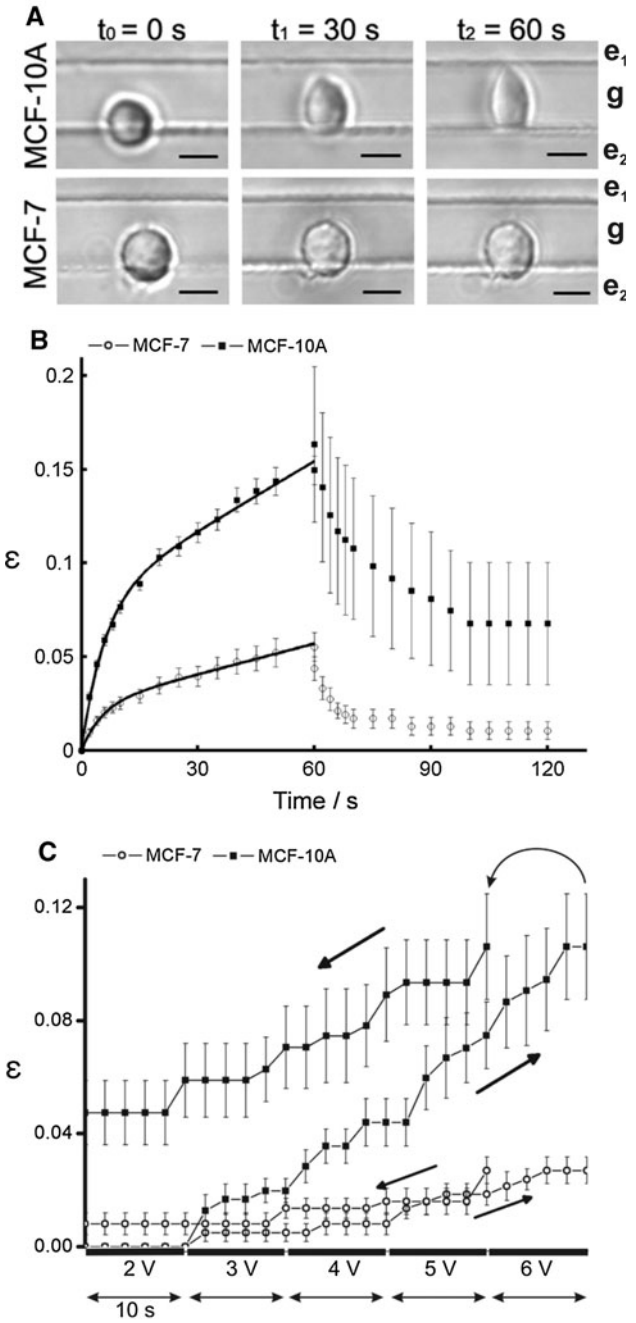

Fig. 2 **a** MCF-10A (*top*) and MCF-7 (*bottom*) cells during elongation due to an electric field in the gap (g) between two electrodes (e_1 and e_2). The difference in stretching after 60 s is easily visible. *Scale bar* 10 μm. **b** Strain response plot of MCF-7 (*open circles*, $n = 40$) and MCF-10A (*full squares*, $n = 37$) cells with constant voltage for load and unload phase (6 and 2 V, respectively) for 60 s per phase. The stretching behavior is clearly different ($p < 0.1\%$), even in the first seconds. The load phase was fitted as described in the text. The relaxation process (60–120 s) was measured in only ten cells each, hence the *error bars* are larger for statistical reasons (smaller sample). **c** Stepwise increase of the voltage every 10 s to 6 V and analogous decrease to 2 V ($n = 10$ each). The *arrows* indicate the step direction. In both cases, **b** and **c**, plastic and elastic deformations are observed

and unloading was 10 s. The graphs show a relaxation behavior of the MCF-10A cells that occurs in approximately equal amounts at each voltage decrease. In the case of MCF-7, the changes are too small to obtain unambiguous information. For both cell types, the measured hysteresis corresponded to the relative strain relaxation of the curves in Fig. 2b.

The DEP force acting on particles is directly proportional to the particle volume. Therefore, even under conditions of equal dielectric properties, the DEP force on cells can differ according to their size. The mean volume of MCF-7 cells (1,920 μm^3) is 47.4% larger than that of the MCF-10A cells (1,303 μm^3). Therefore, the MCF-7 cells experience an increased DEP force. However, they are stretched less. We thus conclude that the observed difference in strain is not due to the difference in size.

The differences in the deformation response between the cancerous and noncancerous cell types are thought to be caused by the structural architecture of their cytoskeleton. Which part of it is mainly responsible for this cell-specific behavior? We performed stretching experiments in the presence of cytoskeleton-active toxins to address this question. Both cell types were treated with either latrunculin A or colchicine, which are inhibitors of actin and microtubule polymerization, respectively (Rotsch and Radmacher 2000; Salmon et al. 1984; Spector et al. 1983). After the latrunculin A treatment, both MCF-7 and MCF-10A cells appeared considerably softer (Fig. 3a), i.e., the strain increased ($P < 0.1\%$). Although the strain of MCF-7 cells increased by approximately 110% and that of MCF-10A cells by 65%, the MCF-7 cells still remained stiffer than the MCF-10A cells ($P \leq 1\%$). In contrast, the colchicine treatment resulted in a softening of both cell types ($P < 0.1\%$), such that the responses of MCF-7 and MCF-10A cells to stretching became indistinguishable ($P > 10\%$ for $t > 2$ s). Our interpretation of these results is that differences in microtubule structures between the two cell types are primarily responsible for their different deformation response.

Using pDEP, the cells come close to the electrodes. As the latter are in an electrolyte, there is a local temperature increase due to joule heating. Cells are close to that region, and viscosity is affected by temperature. However, this does not affect the measurement of the mechanical cell properties beyond the evident elongation observed. Tests on that point employing infrared thermography revealed that under our standard conditions of 6 V and 5 mS/m, warming was only about 0.1 K, mainly due to the low electric conductivity (data not shown). Thus, there is a safe region of electrolyte concentration and voltage. Therefore, viscosity effects due to temperature variations were neglected.

Conclusions

Cells have been stretched between microelectrodes through the application of dielectrophoretic forces. Based on a

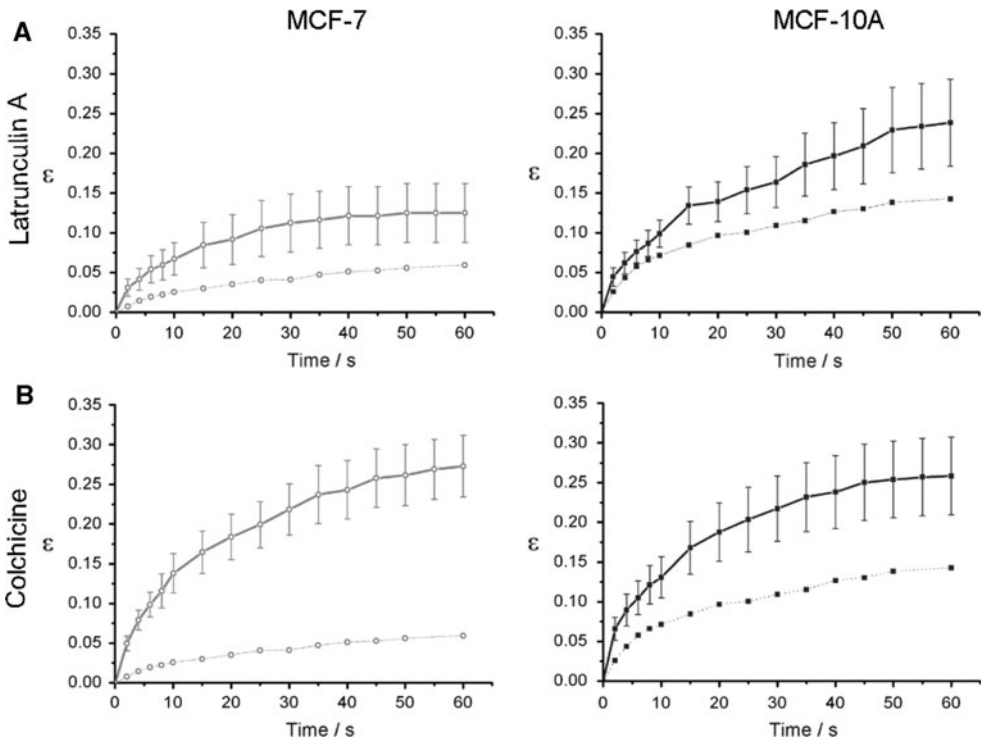

Fig. 3 **a** Effect of latrunculin treatment (1 μM for 1 h). Both cell types ($n = 10$ each) became softer after the treatment. Their respective maximum strain increased by ca. 110 and 65%, respectively. Nonetheless, MCF-7 cells remain stiffer than MCF-10A cells as before. **b** Effect of colchicine treatment (2.5 μM for 2 h). The difference between the MCF-7 ($n = 12$) and MCF-10A ($n = 14$) cells has vanished. This indicates an involvement of microtubules in the different stretching behavior of the cells. For comparison, strain measured in the absence of drugs is shown as *dashed lines* (taken from Fig. 2b, *bars* omitted for clarity). For discussion of statistical significance, see text

relatively small number of two different types of cells, one of cancerous origin (MCF-7) and the other one derived from related noncancerous tissue, reliable data could be obtained that allowed these cells to be unambiguously distinguished. A detailed analysis of the properties of the cells showed that the differences in the stretching response are due to cell-specific mechanical properties of the two cell types. To deduce which parts of the cytoskeleton of the two cell types are mainly responsible for the different stretching behavior, two cytoskeleton-specific toxins have been applied to the cells during the measurements. Addition of latrunculin A, which inhibits actin polymerization, leads to comparable relative changes in the deformation response of the two cell types. The use of colchicine, which blocks microtubule polymerization, softened both cell types, such that they exhibited approximately identical absolute strain values. This indicates that differences in the microtubule structures between the two are the cause for their different responses to dielectrophoretic stretching.

In recent years, the integration of dielectrophoretic elements into lab-on-chip systems has been perfected in many laboratories, such that these devices are now established tools for performing complex cell processing and analysis tasks. In particular, their potential for an automated operation, where many processing steps can be performed in parallel, has attracted much interest. Hence, the design of such chips that allow the screening of mechanical properties of cells and their subsequent sorting with considerable throughput should now be a logical next step forward. If required by more sensitive cell types (e.g., stem cells), the transfer of the cells into the low-electric conductivity medium could then be performed directly on these chips, thus minimizing the exposure of the cells to it.

Acknowledgments This work was supported by the German Research Foundation DFG in the framework of the Priority Programme SPP 1164 (JA 1717/1-2). I.G. is grateful for a scholarship from the Foundation of German Business (SDW). We thank Josef A. Kaes (University of Leipzig, Germany) for helpful discussions. Beate Morgenstern (Fraunhofer IBMT) is acknowledged for cell culture support.

References

Ahn SM, Jeong SJ, Kim YS, Sohn Y, Moon A (2004) Retroviral delivery of TIMP-2 inhibits H-ras-induced migration and invasion in MCF10A human breast epithelial cells. Cancer Lett 207(1):49–57

An J, Lee J, Lee SH, Park J, Kim B (2009) Separation of malignant human breast cancer epithelial cells from healthy epithelial cells using an advanced dielectrophoresis-activated cell sorter (DACS). Anal Bioanal Chem 394:801–809

Binnig G, Quate CF, Gerber C (1986) Atomic force microscopy. Phys Rev Lett 56:930–933

Brown TD (2000) Techniques for mechanical stimulation of cells in vitro: a review. J Biomech 33:3–14

Castellarnau M, Errachid A, Madrid C, Juárez A, Samitier J (2006) Dielectrophoresis as a tool to characterize and differentiate isogenic mutants of *Escherichia coli*. Biophys J 91(10): 3937–3945

Dao M, Limb CT, Suresh S (2003) Mechanics of the human red blood cell deformed by optical tweezers. J Mech Phys Solids 53(2):493–494

Engelhardt H, Sackmann E (1988) On the measurement of shear elastic moduli and viscosities of erythrocyte plasma membranes by transient deformation in high frequency electric fields. Biophys J 54(3):495–508

Engelhardt H, Gaub H, Sackmann E (1984) Viscoelastic properties of erythrocyte membranes in high-frequency electric fields. Nature 307:378–380

Ermolina I, Morgan H (2005) The electrokinetic properties of latex particles: comparison of electrophoresis and dielectrophoresis. J Colloid Interface Sci 285:419–428

Evans EA (1973) New membrane concept applied to the analysis of fluid shear- and micropipette-deformed red blood cells. Biophys J 13(9):941–954

Gimsa J, Marszalek P, Loewe U, Tsong TY (1991) Dielectrophoresis and electrorotation of neurospora slime and murine myeloma cells. Biophys J 60(4):749–760

Guck J, Ananthakrishnan R, Mahmood H, Moon TJ, Cunningham CC, Kaes J (2001) The optical stretcher: a novel laser tool to micromanipulate cells. Biophys J 81(2):767–784

Guck J, Schinkinger S, Lincoln B, Wottawah F, Ebert S, Romeyke M, Lenz D, Erickson HM, Ananthakrishnan R, Mitchell D, Kaes J, Ulvick S, Bilby C (2005) Optical deformability as an inherent cell marker for testing malignant transformation and metastatic competence. Biophys J 88(5):3689–3698

Henderson E, Haydon PG, Sakaguchi DS (1992) Actin filament dynamics in living glial cells imaged by atomic force microscopy. Science 257:1944–1946

Hénon S, Lenormand G, Richert A, Gallet F (1999) A new determination of the shear modulus of the human erythrocyte membrane using optical tweezers. Biophys J 76:1145–1151

Hochmuth RM (2000) Micropipette aspiration of living cells. J Biomech 33(1):15–22

Kim ES, Kim MS, Moon A (2005) Transforming growth factor (tgf)-beta in conjunction with h-ras activation promotes malignant progression of mcf10a breast epithelial cells. Cytokine 29(2): 84–91

Kim YC, Kang JH, Park SJ, Yoon ES, Park JK (2007) Microfluidic biomechanical device for compressive cell stimulation and lysis. Sens Actuators B Chem 128(1):108–116

Kim YC, Park SJ, Park JK (2008) Biomechanical analysis of cancerous and normal cells based on bulge generation in a microfluidic device. Analyst 133:1432–1439

Li QS, Lee GYH, Ong CN, Lim CT (2008) AFM indentation study of breast cancer cells. Biochem Biophys Res Commun 374: 609–613

Lim CT, Dao M, Suresh S, Sow CH, Chew KT (2004) Large deformation of living cells using laser traps. Acta Mater 52(7): 1837–1845

Martin SS, Leder P (2001) Human mcf10a mammary epithelial cells undergo apoptosis following actin depolymerization that is independent of attachment and rescued by bcl-2. Mol Cell Biol 21(19):6529–6536

Mills JP, Qie L, Dao M, Lim CT, Suresh S (2004) Nonlinear elastic and viscoelastic deformation of the human red blood cell with optical tweezers. Mech Chem Biosyst 1:169–180

Park SW, Scapery RA (1999) Methods of interconversion between linear viscoelastic material functions. Part I—a numerical method based on Prony series. Int J Solids Struct 36:1653–1675

Pethig R (1979) Dielectric and electronic properties of biological materials. Wiley, London, pp 186–206

Pethig R, Markx GH (1997) Application of dielectrophoresis in biotechnology. Trends Biotechnol 15(10):426–432

Pohl HA (1978) Dielectrophoresis. Cambridge University Press, Cambridge

Puig-De-Morales M, Grabulosa M, Alcaraz J, Mullol J, Maksym GN, Fredberg JJ, Navajas D (2001) Measurement of cell microrheology by magnetic twisting cytometry with frequency domain demodulation. J Appl Physiol 91(3):1152–1159

Radmacher M, Fritz M, Kacher CM, Cleveland JP, Hansma PK (1996) Measuring the viscoelastic properties of human platelets with the atomic force microscope. Biophys J 70(1):556–567

Rotsch C, Radmacher M (2000) Drug-induced changes of cytoskeletal structure and mechanics in fibroblasts: an atomic force microscopy study. Biophys J 78(1):520–535

Salmon ED, McKeel M, Hays T (1984) Rapid rate of tubulin dissociation from microtubules in the mitotic spindle in vivo measured by blocking polymerization with colchicine. J Cell Biol 99(3):1066–1075

Schnelle T, Mueller T, Fuhr G (1999) Dielectric single particle spectroscopy for measurement of dispersion. Med Biol Eng Comput 37(2):264–271

Spector I, Shochet NR, Kashman Y, Groweiss A (1983) Latrunculins: novel marine toxins that disrupt microfilament organization in cultured cells. Science 219(4584):493–495

Sukhorukov VL, Mussauer H, Zimmermann U (1998) The effect of electrical deformation forces on the electropermeabilization of erythrocyte membranes in low- and high-conductivity media. J Membr Biol 163(3):235–245

Thom F, Gollek H (2006) Calculation of mechanical properties of human red cells based on electrically induced deformation experiments. J Electrostat 64:53–61

Thoumine O, Ott A (1997a) Time scale dependent viscoelastic and contractile regimes in fibroblasts probed by microplate manipulation. J Cell Sci 110(17):2109–2116

Thoumine O, Ott A (1997b) Comparison of the mechanical properties of normal and transformed fibroblasts. Biorheology 34:309–326

Thoumine O, Ott A, Cardoso O, Meister JJ (1999) Microplates: a new tool for manipulation and mechanical perturbation of individual cells. J Biochem Biophys Methods 39:47–62

Tuszyński JA, Trpišová B, Sept D, Brown JA (1997) Selected physical issues in the structure and function of microtubules. J Struct Biol 118:94–106

Van Vliet KJ, Bao G, Suresh S (2003) The biomechanics toolbox: experimental approaches for living cells. Acta Mater 51(19): 5881–5905

Wang N, Butler JP, Ingber DE (1993) Mechanotransduction across the cell surface and through the cytoskeleton. Science 260:1124–1127

Wottawah F, Schinkinger S, Lincoln B, Ananthakrishnan R, Romeyke M, Guck J, Kaes J (2005) Optical rheology of biological cells. Phys Rev Lett 94(9):98–103